

Cluster-based control of nonlinear dynamics

Eurika Kaiser · Bernd R. Noack · Andreas Spohn ·
Louis N. Cattafesta · Marek Morzyński

Received: date / Accepted: date

Abstract The ability to manipulate and control fluid flows is of great importance in many scientific and engineering applications. Here, a cluster-based control framework is proposed to determine optimal control laws with respect to a cost function for unsteady flows. The proposed methodology frames high-dimensional, nonlinear dynamics into low-dimensional, probabilistic, linear dynamics which considerably simplifies the optimal control problem while preserving nonlinear actuation mechanisms. The data-driven approach builds upon a state space discretization using a clustering algorithm which groups kinematically similar flow states into a low number of clusters. The temporal evolution of the probability distribution on this set of clusters is then described by a Markov model. The Markov model can be used as predictor for the ergodic probability distribution for a particular control law. This probability distribution approximates the long-term behavior of the original system on which basis the optimal control law is determined. The approach is applied to a separating flow dominated by the Kelvin-Helmholtz shedding.

Keywords Flow control · Markov model · cluster analysis · Liouville equation · flow separation · feedback control

1 Introduction

Controlling complex dynamical systems such as fluid flows is of great importance in science and engineering. Examples include drag reduction for greener transport systems, lift increase on airfoils, stabilization of combustion processes, reduction of pollutants from chemical processes, and efficiency increase of energy harvesting systems like wind turbines, to name a few. Closed-loop control which translates the continuously monitored system state into control actions is a particularly promising direction. We refer to [11] for a recent review on closed-loop control.

Of particular interest in control applications are certain statistical flow properties like the average drag or lift which shall be mitigated or increased, respectively. However, their computation from trajectories may

E. Kaiser
University of Washington, Mechanical Engineering Department, Seattle, WA 98195, USA
E-mail: eurika.kaiser@gmail.com

E. Kaiser · B. R. Noack · A. Spohn
Institut PPRIME, UPR 3346 CNRS – Université de Poitiers – ENSMA, F-86961 Futuroscope Chasseneuil, France

B. R. Noack
LIMSI-CNRS, UPR 3251, F-91405 Orsay cedex, France, France
Technische Universität Braunschweig, D-38108 Braunschweig, Germany

L. N. Cattafesta
Florida State University, Florida Center for Advanced Aero-Propulsion, Tallahassee, FL 32310, USA

Marek Morzyński
Poznan University of Technology, Piotrowo 3, 60-965 Poznan, Poland

be misleading for several reasons. The time average is generally computed over a limited time span which makes it sensitive to transient behavior and biased as the trajectory may reside only in a confined state space region. Thus, very long integration times are required to ensure that the time average is good. However, even without noise and external disturbances, small uncertainties in initial or boundary conditions may doom a deterministic system unpredictable. A well-studied example is the chaotic Lorenz system introduced by E. N. Lorenz [26], a simplified model for atmospheric convection with known sensitivity to initial conditions.

Average properties over long time spans lead naturally to invariant probability measures on the attractor, i.e. these measures stay the same after transformation of the attractor. Ergodic measures, a sub-class of invariant measures, are of particular interest as for those time averages are equal to space averages according to Birkhoff's ergodic theorem [24]. This assumption is often assumed when analyzing fluid flows: These flows are assumed to be ergodic, i.e. in the sense that they are statistically reproducible, allowing to compute the statistical properties from ensemble averages. In this study, the system's dynamics are modelled in terms of a Markov model, particularly a cluster-based reduced-order model (CROM) [23]. This simplification allows to compute many (statistical) properties exactly which are often good estimators for the analogous properties of the original system [16]. As a consequence of Birkhoff's ergodic theorem, controlling such statistical properties is strongly related to the control of the ergodic measure on the attractor.

The Markov model is a linear evolution equation for a probability distribution in the state space. Such evolution equations can be derived from the Navier-Stokes equation, starting with the linear Liouville equation of a suitable probability space. The Hopf [21] formalism for the Navier-Stokes equation is a prominent example. A simpler version constitutes the Liouville equation for a Galerkin system. The reader is referred to [32] for a detailed discussion. CROM is closely aligned with closure schemes, in which a stable fixed point represents the ergodic measure for the unsteady attractor in velocity space. While the control of a Liouville equation has not found much attention in fluid dynamics yet, it is studied widely in other fields such as atomic physics [31], biology [9], and robotics [8,27]. An extensive study on the optimal control of the Liouville equation is provided in [7]. The control of the Liouville equation can be interpreted as the manipulation of a particular system using a single controller over repeated realizations which correspond to different initial conditions. Thus, the control of the Liouville equation is a promising direction for systems that exhibit uncertainties in initial conditions and system parameters, e.g. due to disturbances.

The present work is outlined as follows: In Sec. 2, the cluster-based control methodology is described. The approach is applied to the benchmark problem of a separating flow over a backward-facing, smoothly contoured ramp which results are presented in Sec. 3. The main results are summarized and discussed in Sec. 4. Details on the empirical estimation of the Markov model and its properties are given in Appendix A. In Sec. C, a technique for visualizing the similarity of control laws is briefly explained.

2 Cluster-based control methodology

2.1 Problem formulation

In this work, we are concerned with identifying a probabilistic low-order representation of the deterministic, fully nonlinear dynamics and deriving optimal control laws with respect to an objective function. Generally, a dynamical system is represented as

$$\frac{d}{dt}\mathbf{a}(t) = \mathbf{F}(\mathbf{a}(t), \mathbf{b}(t)) \quad (1)$$

where the vector \mathbf{a} denotes the system state and vector \mathbf{b} is the control input at time t , and \mathbf{F} is the nonlinear propagator for the system state \mathbf{a} . We assume a full-state feedback ansatz for the control in the form

$$\mathbf{b} = K(\mathbf{a}) \quad (2)$$

where K represents the control law that maps states \mathbf{a} into control actions \mathbf{b} . In optimal control, one seeks to determine an optimal control law K^{opt} which minimizes a cost function. The cost function, generally a function of the system state \mathbf{a} and the control \mathbf{b} , defines the control objective through a performance measure and penalty function evaluating the cost of the applied control, and incorporates additional

constraints. In flow control, the average drag or lift are often of interest. Let $h(\mathbf{a})$ be a function measuring a quantity of interest, e.g., the drag, along the trajectory $\mathbf{a}(t)$. For ergodic behavior, the temporal average $\langle h(\mathbf{a}) \rangle_T := \lim_{T \rightarrow \infty} \frac{1}{T} \int_0^T h(\mathbf{a}(t)) dt$ can be represented in terms of the spatial average $\langle h(\mathbf{a}) \rangle_\Omega := \int_\Omega h(\mathbf{a}) p(\mathbf{a}) d\mathbf{a}$ which is naturally defined by the probability density function (p.d.f.) $p(\mathbf{a})$. The average cost function can then be formulated as

$$J_K = \mathbb{E}^\infty [j(\mathbf{a}, \mathbf{b}) |_{\mathbf{b}=K(\mathbf{a})}] = \int_\Omega j(\mathbf{a}, \mathbf{b}) |_{\mathbf{b}=K(\mathbf{a})} p^\infty(\mathbf{a}) d\mathbf{a} \quad (3)$$

where $j(\mathbf{a}, \mathbf{b})$ is the local cost function, \mathbb{E}^∞ is the expectation operator assuming transients have decayed, and $p^\infty(\mathbf{a})$ is the asymptotic, i.e. long-run, p.d.f. The control design task is to determine K^{opt} such that the p.d.f. $p^\infty(\mathbf{a})$ is as close as possible to a desired density for which the average cost J_K is minimized. The evolution of the p.d.f. is prescribed by a Liouville equation associated with the dynamical system (1),

$$\frac{\partial}{\partial t} p(\mathbf{a}, t) + \nabla_{\mathbf{a}} \cdot [p(\mathbf{a}, t) \mathbf{F}(\mathbf{a}, \mathbf{b})] = 0. \quad (4)$$

While the dynamical system (1) prescribes the evolution of a single trajectory in the state space, the Liouville equation (4) is a linear equation for the p.d.f. describing the distribution of a swarm of trajectories in the state space. Linked to the Liouville equation (4) is the Perron-Frobenius operator P_t [24], a linear evolution operator, that maps the p.d.f. forward in time,

$$p(\mathbf{a}, t) = P_t p(\mathbf{a}(0)) \quad (5)$$

with $P_t := \exp(tL)$ where $L := -\nabla_{\mathbf{a}} \cdot (p(\mathbf{a}, t) \mathbf{F}(\mathbf{a}, \mathbf{b}))$ is the Liouville operator. An invariant (or long-term) p.d.f. $p^\infty(\mathbf{a})$ constitutes a solution to the fixed-point equation $p(\mathbf{a}) = P_t p(\mathbf{a})$ for all $t \geq 0$. Note that a unique solution is not expected and there can be many or even infinitely many invariant p.d.f.s. For instance, if the dynamical system (1) possesses a fixed point \mathbf{a}^* , the invariant density will be a peak supported over the fixed point, i.e. $p^\infty(\mathbf{a}) = \delta(\mathbf{a} - \mathbf{a}^*)$ where δ is the Dirac delta function. If (1) exhibits a periodic limit cycle, the invariant density is the sum of delta functions supported over the points \mathbf{a}_i^* , $i = 1, \dots, N_{lc}$, constituting the limit cycle, i.e. $p^\infty(\mathbf{a}) = \sum_{i=1}^{N_{lc}} \delta(\mathbf{a} - \mathbf{a}_i^*)$. If (1) is a chaotic dynamical system, it consists of infinitely many limit cycles and therefore of infinitely many invariant densities. the reader is referred to [6] for more details on this topic.

2.2 Discrete coarse-graining of state space

Let \mathcal{A}_i , $i = 1, \dots, N_a$, be a discretization of the state space such that $\mathcal{A} = \cup_{i=1}^{N_a} \mathcal{A}_i$ with $\mathcal{A}_i \cap \mathcal{A}_j = \emptyset$ for $i \neq j$. Here, a data-driven partitioning method is pursued as outlined in App. A. which yields a discrete number of clusters \mathcal{A}_i with centroids \mathbf{A}_i which are the as representative states of each cluster. Each state $\mathbf{a}(t)$ is connected to a symbol α representing the cluster \mathcal{A}_α to which $\mathbf{a}(t)$ belongs. Let the measurable equation, which maps the continuous state \mathbf{a} to a discrete symbol α , be defined by

$$\alpha(t) = \chi(\mathbf{a}(t)) \in \{1, 2, \dots, N_a\}. \quad (6)$$

The coarse-grained inverse mapping is defined by

$$\mathbf{a}^\circ(t) = \mathbf{A}_{\chi(\mathbf{a}(t))} \quad (7)$$

approximating the continuous state \mathbf{a} by its closest cluster centroids, e.g., $\alpha = 1$ and $\mathbf{a}^\circ = \mathbf{A}_1$ if $\mathbf{a} \in \mathcal{A}_1$. The superscript $^\circ$ refers to the discrete-state approximation. The inverse operation is associated with a loss of information due to the coarse-graining process. Let the characteristic function be defined by

$$\chi_i(\mathbf{a}) = \begin{cases} 1 & \text{if } \mathbf{a} \in \mathcal{A}_i, \\ 0 & \text{if } \mathbf{a} \notin \mathcal{A}_i \end{cases} \quad \text{or} \quad \chi_i(\mathbf{a}) = \delta(\chi(\mathbf{a}) - i) \quad (8)$$

where δ is the Kronecker delta. The full-state feedback ansatz for the control is then

$$\mathbf{b}^\circ = K(\mathbf{a}^\circ) = K(\mathbf{A}_{\chi(\mathbf{a})}) = \kappa(\alpha) = \sum_{i=1}^{N_a} \mathbf{B}_i \chi_i(\mathbf{a}). \quad (9)$$

As a result of the discretization, the control \mathbf{b} is piecewise constant where \mathbf{B}_i are vectors of real numbers and denote the control applied in cluster \mathcal{A}_i . The control law κ , that maps discrete states \mathbf{A}_i with symbols α into control actions \mathbf{b}° , is considered stationary here, i.e. \mathbf{B}_α for a cluster α remains constant for all times. The optimal control law κ^{opt} minimizes the average cost function

$$J_\kappa = \mathbb{E}^\infty [j^\circ(\alpha, \mathbf{b})|_{\mathbf{b}=\kappa(\alpha)}] = \sum_{i=1}^{N_a} j^\circ(i, \kappa(i)) p_i^{\circ, \infty} \quad (10)$$

with the local cost function $j^\circ(\alpha, \mathbf{b})|_{\mathbf{b}=\kappa(\alpha)}$ evaluating the cost for the currently prevailing cluster α and the control input B_α applied in this cluster. The vector $\mathbf{p}^{\circ, \infty}$ is the discrete asymptotic probability distribution for $t \rightarrow \infty$. This constitutes the solution to the fixed-point equation associated with the discrete-state Markov model

$$\frac{d}{dt} \mathbf{p}^\circ(t) = \mathbf{P}_\kappa^\circ \mathbf{p}^\circ(t). \quad (11)$$

This equation describes the temporal evolution of the probability vector $\mathbf{p}^\circ = [p_1^\circ, \dots, p_{N_a}^\circ]^T$ where p_i is the probability that the trajectory $\mathbf{a}(t)$ resides in cluster \mathcal{A}_i . The matrix \mathbf{P}_κ° prescribes the dynamics on the coarse-grained state space following a particular control law κ .

The Markov model (11) can be derived from (4) using Ulam's method [35, ?] which is classically used in dynamical systems to determine a finite-rank approximation of the Perron-Frobenius operator (5). Ulam's method involves a Galerkin projection of the Liouville equation (4) onto a particular set of basis functions. Recently, [23] showed that the cluster-based reduced-order modeling approach can be interpreted as a generalization of Ulam's method.

2.3 Discrete-time, discrete-state formulation

A further discretization level based on the time is considered. Let the floor function be defined as $\lfloor t \rfloor := \max\{l \in \mathbb{Z} \mid l \leq t\}$ [22]. A polymorphism for continuous-time and discrete-time variables is pursued for the purpose of a better readability. The measurement equation in analogy to (6) is given by

$$\alpha^t = \chi(\mathbf{a}(\lfloor t \rfloor)) \in \{1, 2, \dots, N_a\} \quad (12)$$

for discrete times t , the superscript t is an index corresponding to multiple of Δt , and where χ is the characteristic function as introduced above. The inverse discrete-time, coarse-grained mapping is given by

$$\mathbf{a}^{\bullet, t} = \mathbf{A}_{\chi(\mathbf{a}(\lfloor t \rfloor))}. \quad (13)$$

The superscript $^\bullet$ refers here to the discrete-state, discrete-time representation of quantities. The full-state feedback ansatz for the control becomes

$$\mathbf{b}^\bullet = K(\mathbf{a}^\bullet) = K(\mathbf{A}_{\chi(\mathbf{a}(\lfloor t \rfloor))}) = \kappa(\alpha) \quad (14)$$

realizing the time-delay. The optimal control law κ^{opt} shall minimize the average cost function

$$J_\kappa = \mathbb{E}^\infty [j^\bullet(\alpha, \mathbf{b})|_{\mathbf{b}=\kappa(\alpha)}] = \sum_{i=1}^{N_a} j^\bullet(i, \kappa(i)) p_i^{\bullet, \infty} \quad (15)$$

with local cost function $j^\bullet(\alpha, \mathbf{b})|_{\mathbf{b}=\kappa(\alpha)}$. The asymptotic probability vector $\mathbf{p}^{\bullet, \infty}$ is a solution to the fixed-point equation of the discrete-state, discrete-time Markov model which describes consecutive distributions by the iteration formula

$$\mathbf{p}^{\bullet, t+1} = \mathbf{P}_\kappa^\bullet \mathbf{p}^{\bullet, t}, \quad t = 0, 1, 2, \dots \quad (16)$$

with the cluster transition probability matrix $\mathbf{P}_\kappa^\bullet$ prescribing the dynamics following a particular control law κ .

2.4 Control design using CROM

In the following, the discrete-state, discrete-time formulation of Sec. 2.3 is considered and the superscript \bullet is dropped. We consider single-output control laws of the form

$$\kappa(\alpha) = \sum_{i=1}^{N_a} B_i \chi_i(\mathbf{a}) = \sum_{i=1}^{N_a} \tilde{\kappa} \sin(\omega_p t) \chi_i(\mathbf{a}) \quad (17)$$

where $\tilde{\kappa}$ denotes a fixed amplitude for the actuation, the cluster-dependent control values become scalars $B_1 = B_2 = \dots = B_{N_a} = \tilde{\kappa} \sin(\omega_p t)$, and $\chi_i(\mathbf{a})$ is the characteristic function defined in (8). As $\chi_i(\mathbf{a})$ assumes values 0 or 1, the periodic actuation is turned off or on, respectively, depending on the prevailing cluster $\alpha = i$. Thus, the control law $\kappa(\alpha)$ is uniquely determined by the characteristic function $\chi_i(\mathbf{a})$.

Let be assumed that the state space is discretized into $N_a = 10$ clusters. Since $\chi_i(\mathbf{a})$ can only assume two possible values and the number of clusters is fixed, there exists a fixed number of possible control laws defined by all possible combinations of '0's and '1's. Let the control law be represented by a string of '0's and '1's of length N_a . The number of '1's in this string shall be denoted as N_v . The total number of combinations of how N_v '1's can be arranged in this string, i.e. on N_a clusters, is given by $\sum_{0 \leq N_v \leq N_a} C(N_a, N_v) = \sum_{0 \leq N_v \leq N_a} \binom{N_a}{N_v} = 2^{N_a}$. For the given example of $N_a = 10$ clusters, the total number of control laws is thus $\sum_{0 \leq N_v \leq 10} \binom{10}{N_v} = 2^{10} = 1024$:

$$\kappa^0(\alpha) = B_{0000000000} = 0, \quad (18a)$$

$$\kappa^1(\alpha) = B_{0000000001} = B_1 \delta(\alpha - 1), \quad (18b)$$

$$\vdots$$

$$\kappa^{386}(\alpha) = B_{0110000010} = B_2 \delta(\alpha - 2) + B_8 \delta(\alpha - 8) + B_9 \delta(\alpha - 9), \quad (18c)$$

$$\vdots$$

$$\kappa^{1023}(\alpha) = B_{1111111111} = \sum_{i=1}^{N_a} B_i \delta(\alpha - i). \quad (18d)$$

where B_{xxxxxxxx} with $x \in \{0, 1\}$ refers to the string representing the control law. The control design task consists of determining the control law that minimizes the average cost function (15). For any control law $\kappa(\alpha)$ (or $\kappa^l(\alpha)$, respectively) such a cost J_κ can be simply evaluated,

$$J_\kappa = \sum_{i=1}^{N_a} j(i, \kappa(i)) p_{\kappa, i}^\infty = \sum_{i=1}^{N_a} j(i, \kappa(i)) p_{\kappa, i}^{*1}, \quad (19)$$

exploiting that the dynamics introduced by a control law $\kappa(\alpha)$ are described by \mathbf{P}_κ . This is a critical enabler for the control design as it allows the prediction of the invariant probability distribution \mathbf{p}_κ^∞ by the eigenvector \mathbf{p}_κ^{*1} associated with the dominant eigenvalue λ_κ^1 of \mathbf{P}_κ (see appendix B). Having determined J_κ for all κ , the optimal control law is then given by

$$\kappa^{opt}(\alpha) = \arg \min_{b=\kappa(\alpha)} J_\kappa \quad \text{with} \quad J^{opt} = \min_{b=\kappa(\alpha)} J_\kappa. \quad (20)$$

3 Control of a separating flow over a smooth ramp

3.1 Flow configuration and numerical simulation

The two-dimensional flow is described by a Cartesian coordinate system in which the location vector is denoted by $\mathbf{x} = (x, y)^T$ where x is in flow direction and y is the direction perpendicular to x . The two-dimensional velocity vector is denoted by $\mathbf{u}(\mathbf{x}, t) := (u, v)^T$ where u and v are the velocities in x - and

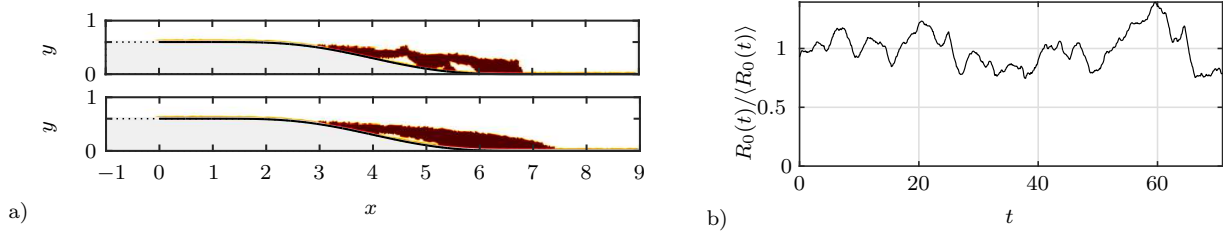


Fig. 1 Recirculation area of (a, top) an instantaneous velocity snapshot and (a, bottom) the mean flow, and (c) time series of the normalized recirculation area for the uncontrolled flow.

y -direction, respectively, and t denotes the time. The pressure is represented by P . The non-dimensionalized Navier-Stokes and continuity equations are

$$\begin{aligned} \partial_t \mathbf{u} + \nabla \cdot (\mathbf{u} \mathbf{u}) &= -\nabla P + \frac{1}{Re} \Delta \mathbf{u} + \mathbf{G} b, \\ \nabla \cdot \mathbf{u} &= 0 \end{aligned} \quad (21)$$

where $Re = U_\infty L / \nu$ is the Reynolds number and \mathbf{G} is a steady local force field in y -direction. The function b is the time-dependent control input amplitude and has compact support in a circular region. It is centered at $x = 1$ and the y -position is chosen such that the circular region is mostly inside the boundary layer. The computational domain Ω for the flow comprises

$$\Omega := \{(x, y) : -1 \leq x \leq 10, f(x) \leq y \leq 2.6\}. \quad (22)$$

The domain is discretized as mixed Taylor-Hood elements [20] on an unstructured triangular mesh comprising 8567 nodes with increased resolution around the leading edge, in the boundary layer and in the shear layer region. A quadratic finite-element method formulation is used to discretize the evolution equations with no-slip boundary on the ramp and stress-free outflow. A detailed description of the solver can be found in [30, 1]. A rectangular velocity profile $\mathbf{U}_\infty := \mathbf{u}(x = 1, y) = (1, 0)^T$ is used as inflow. The numerical time step is 0.005 and the sampling period of the snapshots is 20, i.e. $\Delta t = 0.1$. The topography of the smooth ramp is described by a polynomial shape of order 7 [33, 2]. Due to an adverse pressure gradient induced by the curvature of the ramp, the flow separates from the wall leading to a large recirculation area and the development of a convectively unstable free shear layer. It gives rise to the Kelvin-Helmholtz instability by which two-dimensional perturbations are spatially amplified eventually roll up into vortices [18]. This recirculation area is characterized by fluid moving in the opposite direction of the flow. High pressure drag and low lift forces are associated with large recirculation areas on airfoils. In this study, the objective is to reduce the recirculation area in order to attenuate the pressure drag. The mean recirculation area $\langle R(t) \rangle$ is defined by

$$\langle R(t) \rangle = \frac{1}{T_2 - T_1} \int_{T_1}^{T_2} \int_{\Omega_R} H(-u(\mathbf{x}))(t) \, d\mathbf{x} \, dt \quad (23)$$

where H denotes the Heaviside function, Ω_R is the chosen region for evaluation, and the limits for the temporal integration are chosen such that the transient is excluded, i.e. $T_1 = 25 \approx 4.4 T_{sh}$ and $T_2 - T_1 = 70 \approx 7.92 T_{sh}$ with the shedding period $T_{sh} = 1/f_{sh}$ of the uncontrolled flow. The estimation of the recirculation area is an approximation assuming that the recirculation area corresponds to those regions where the streamwise velocity component is negative. The average cost function to assess the performance of the control is defined by

$$J = \frac{\langle R(t) \rangle}{\langle R_0(t) \rangle} \quad (24)$$

normalized by the mean recirculation area $\langle R_0(t) \rangle$ of the uncontrolled flow. An instantaneous and mean plot of the recirculation area of the uncontrolled flow are shown in figure 1.

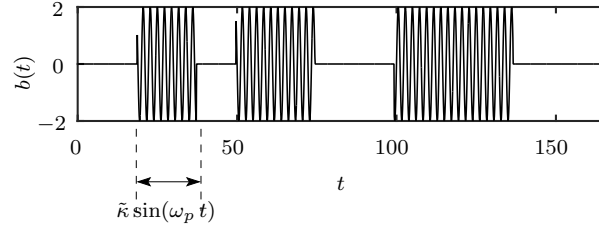


Fig. 2 Actuation signal for model identification switching between phases where $b = \tilde{\kappa} \sin(\omega_p t)$ and $b = 0$.

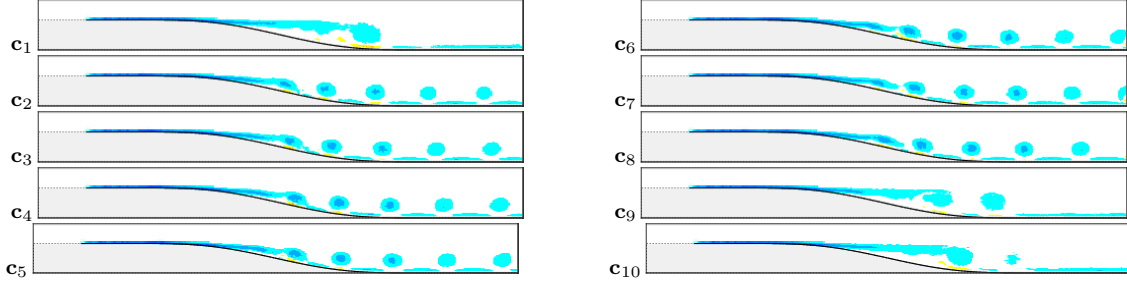


Fig. 3 Cluster vorticity centroids $\mathbf{c}_i(\mathbf{x}) = \nabla \times (1/n_i \sum_{\mathbf{a}^m \in \mathcal{A}_i} \mathbf{u}^m(\mathbf{x}))$ for each cluster \mathcal{A}_i .

3.2 Control results

We consider feedback control laws κ of the form presented in (17) where the periodic excitation is turned on ($\chi_\alpha(\mathbf{a}) = 1$) or off ($\chi_\alpha(\mathbf{a}) = 0$) depending on the prevailing cluster α . A suitable frequency for ω_p can be easily determined using open-loop periodic forcing and selecting the frequency for which the recirculation area has decreased most. For the considered flow simulation, this frequency has been determined as $f_p = 0.45$. Thus, the control law is based on the best periodic excitation exploiting that this frequency is known to be effective. The system state $\mathbf{a} := [a_1, \dots, a_N]^T$ is given by

$$\mathbf{a}(t_m) = \int_{\Omega} \Phi_N^T \mathbf{u}^m(\mathbf{x}) d\mathbf{x} \quad (25)$$

projecting the instantaneous velocity snapshot \mathbf{u}^m onto the first $N_{pod} = 10$ proper orthogonal decomposition [19] (POD) modes $\mathbf{u}_i^p(\mathbf{x})$ constituting the columns of $\Phi_N := [\mathbf{u}_1^p, \dots, \mathbf{u}_N^p]$. These POD modes are computed from a snapshot ensemble sampled of a flow under periodic excitation with $f_p = 0.45$.

The data for the cluster and model identification is collected from applying the actuation signal (see figure 2), which comprises time spans where the control is either turned on or off. The temporal signal of the POD coefficient vector \mathbf{a} is computed from the acquired snapshot set according to (25). The state space is discretized by applying an unsupervised clustering algorithm (see App. A) to the data ensemble $\{\mathbf{a}^m\}_{m=1}^M$ with the number of clusters $N_a = 10$. The cluster centroids based on the vorticity of the snapshots belonging to each cluster are displayed in figure 3. Most centroids, $i = 2, 3, 4, 5, 6, 7, 8$, represent the lock-in state when periodically exciting the flow. The remaining centroids, $i = 1, 9, 10$, are associated with the uncontrolled flow. Transient states are not resolved.

A local cost function $j(i)$ is associated with each cluster \mathcal{A}_i

$$j(i) = \frac{1}{n_i} \sum_{\mathbf{a}^m \in \mathcal{A}_i} R(t_m). \quad (26)$$

in terms of the recirculation area averaged over the snapshots belonging to cluster \mathcal{A}_i . The desirability of a particular cluster is thus represented by this cost taking into account the control objective (compare Sec. 3.1), while the control input is not penalized here. The control-dependent transition probabilities are computed

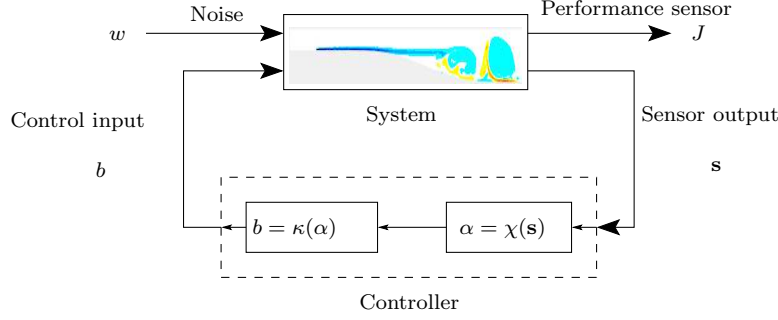


Fig. 4 Schematic of feedback control loop.

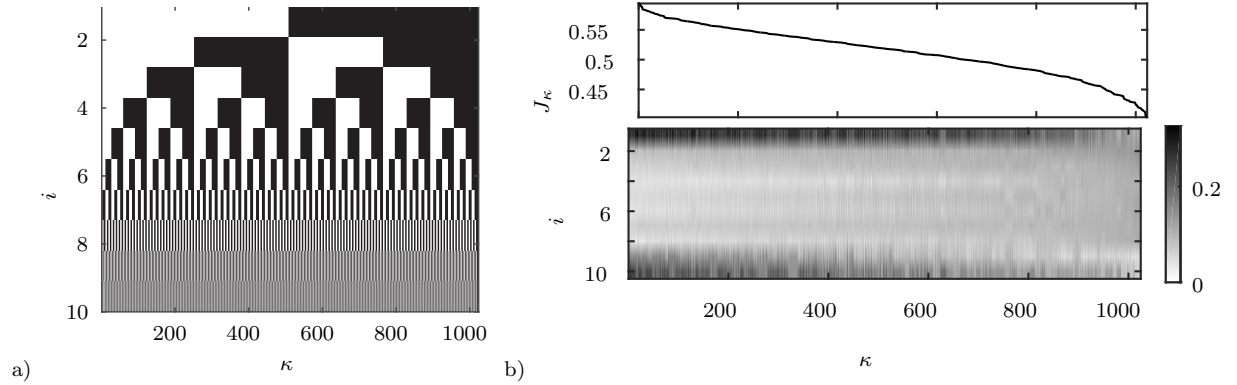


Fig. 5 Optimal control law: (a) set of control laws κ^l , $l \in \{1, \dots, 1024\}$, (b, top) their average cost J_κ (see (19)), and (b, bottom) the eigenvector \mathbf{p}^{*1} corresponding to the dominant eigenvalue λ_1 of the associated transition matrix \mathbf{P}_κ . The symbols \square and \blacksquare depict the control state 'off', i.e. $\chi_\alpha(\mathbf{a}) = 0$, or 'on', i.e. $\chi_\alpha(\mathbf{a}) = 1$, respectively. Note that the control laws in both figures in (b) are sorted according to descending costs J_κ . Thus, the best control law corresponds to the right most control law.

according to (29) in App. B and are used to construct the cluster transition matrices \mathbf{P}_κ prescribing the dynamics under control law κ .

The feedback control loop is displayed in figure 4. A sensor reading \mathbf{s} is fed back to the controller in which first the prevailing cluster α is computed and then the control input b is determined based on the control law $\kappa(\alpha)$. Here, full-state information is assumed, i.e. $\mathbf{s} = \mathbf{a}$. A realistic system is generally affected by noise which is neglected in this study. A sensor measures the performance J of the control law with regard to the control objective. The set of control laws to be evaluated is shown in figure 5(b). The abscissa depicts the control laws $\kappa^l(\alpha)$ and the ordinate corresponds to the cluster index i , which is selected by the prevailing cluster α . The asymptotic probability vectors $\mathbf{p}_\kappa^\infty \forall \kappa$ originating from the dynamics prescribed by \mathbf{P}_κ can be predicted by the corresponding eigenvector \mathbf{p}_κ^{*1} (see figure 5(b, bottom)). The associated average cost (19) is displayed above in figure 5(b, top). The optimal control law $\kappa^{opt} = B_{0010101111}$ as determined by (20) is the right most. The left most probability vectors are clearly in favor of cluster 1, 9 and 10, and have comparably low probabilities in the remaining clusters. For these control laws, the flow remains mostly in the clusters corresponding to the uncontrolled flow (compare figure 3). In contrast, for those probability vectors on the right-hand side, the condition is reversed: the probabilities of clusters 1, 9 and 10 are much lower and those of the remaining clusters have increased. Thus, these control laws direct the flow to clusters associated with smaller recirculation areas.

This analysis is based on the prediction of the models \mathbf{P}_κ . In addition, all control laws are evaluated in the numerical simulation. The mean input energy is defined by $\langle b^2(t) \rangle = \frac{1}{T_2 - T_1} \int_{T_1}^{T_2} b^2(t) dt$ based on the applied actuation signal b to assess the required control effort. A Pareto diagram of the control results is shown in figure 6(a). The axes of figure 6(a) are normalized based on the mean recirculation area of the uncontrolled flow and the mean input energy of the open-loop periodic forcing. The periodically forced flow

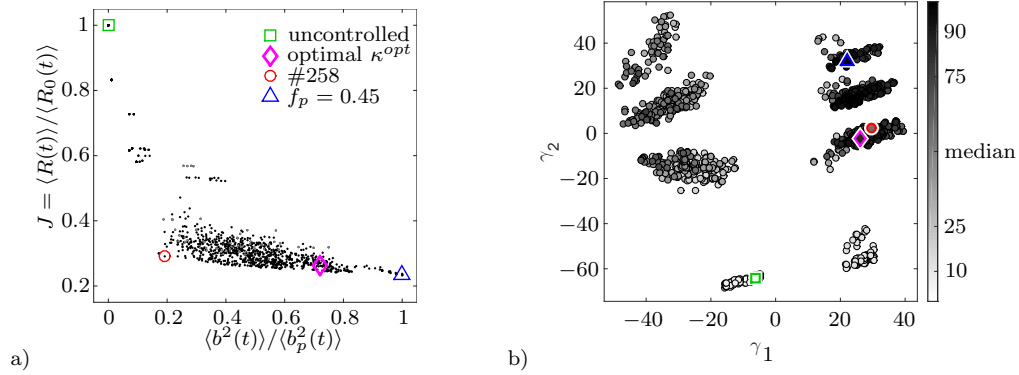


Fig. 6 Control law evaluation: (a) Pareto diagram of control laws and (b) two-dimensional visualization of the control laws based on their similarity and colored by the percentile rank of their performance J .

has clearly the smallest recirculation area (23%). The optimal control law κ^{opt} produces a slightly larger recirculation area (26%). Interestingly, the optimal control law yields a comparable J while considerably decreasing the required input energy by 28%. There is a trade-off: the recirculation area cannot be reduced without increasing the required input energy. If these effects are weighted evenly, the best trade-off is achieved by control law #258 ($B_{0100000010}$) with a recirculation area corresponding to 29% and a reduction of the input energy by 81%. Note that this control law can be attributed to the synchronization of the flow to recurring peaks in the actuation with frequency f_p . Finally, the similarity of the control laws is analyzed. In figure 6(b), a two-dimensional plot is displayed where each circle corresponds to a particular control law κ^l . The distance between these circles depicts their respective similarity as defined in (33) in App. C. The color of the circles depicts the percentile rank of J associated with a particular control law, e.g. 90 and higher correspond to the best 10% of control laws. The percentile rank is computed using the nearest rank method. The control laws are arranged in several groups: two lower bright groups corresponding to poorly performing control laws, three large groups with mixed performance on the left-hand side, and three groups of similar size on the right-hand side with majoritarily better performance. Interestingly, κ^{opt} and #258 belong to the same group while κ^{opt} has a more similar performance with periodic forcing. The grouping of the clusters is influenced by the state space discretization. For example, the uncontrolled flow exhibits mainly clusters 1, 9, 10 and with negligible probability clusters 2 and 3. Any control law of the form $B_{000xxxx00}$, where x can be any control value, must be similar to $b(t) = 0 \forall t$ and perform like the uncontrolled flow, and thus belong to the same group in figure 6(b). Further analysis is required to clarify the exact origin of the grouping.

4 Conclusions

The present study proposes a cluster-based control strategy for the determination of optimal control laws for unsteady fluid flows. This framework builds upon a cluster-based reduced-order model (CROM) which translates high-dimensional, nonlinear dynamics into low-dimensional, probabilistic dynamics. The control problem is formulated as a combinatorial optimization problem for the average cost. The ability to find the optimal control law in an unsupervised manner highlights the generic applicability of the framework to other dynamical systems.

The approach is demonstrated for a separating flow over a smooth ramp with the aim to reduce the mean recirculation area. An important observation is the trade-off between the recirculation area and the required control effort. One cannot be decreased without increasing the other. Intriguingly, while the number of clusters is too low to resolve the transition process, considerably reductions in the input energy can be achieved through the optimal control law while yielding a similarly reduced recirculation area with respect to periodic excitation. One particularly efficient control law is attributed to the synchronization of the flow to recurring peaks in the actuation. Similarly to sinusoidal forcing, the flow exhibits a lock-in state with the actuation frequency. As a consequence, the flow separates later with much smaller vortices shedding closely along the wall.

Discrete formulations like the proposed cluster-based control framework face the curse of dimensionality [3] where the high-dimensionality of the problem as a result of the discretization prevents an exhaustive search for the optimal solution. Model-free extensions like approximate dynamic programming exist to approximate the optimal cost function, e.g. using function approximators [4] or by successively improving the cost function through learning [34]. Alternatively, other optimization algorithms for the exploration of the solution space could be employed in order to circumvent this difficulty. For example, genetic algorithm, an evolutionary optimization method classically used for parameter optimization [36], aims to find the optimal solution by generating and evolving a set of candidate solutions based on the natural selection process.

The online-capability of control strategies is critical for their application in realistic configurations. For a low number of sensors, e.g. of $\mathcal{O}(1) - \mathcal{O}(10^3)$, the involved calculations when applying the control law are sufficiently fast. If the flow state is based on velocity field measurements typically of $\mathcal{O}(10^5) - \mathcal{O}(10^7)$, the clustering algorithm is applied in the POD space as similarly done in this study. Then, the method will benefit from recent advances in compressed sensing [10] to find optimal sparse sensors in the high-dimensional velocity space that determine the instantaneous cluster affiliation.

Flow control has a long tradition in scientific and engineering applications. We believe that recent advances in data science [13, 12] and machine learning techniques [15, 17] for flow control will be transformative in the coming years. The cluster-based control framework, that is purely data-driven and determines optimal control laws in an unsupervised manner, contributes to this direction. The proposed approach offers a promising new path for controlling the ergodic measure on the attractor taking into account nonlinear actuation mechanisms.

Acknowledgements The authors acknowledge the funding and excellent working conditions of the project Separation Control - From passive to closed-loop design (SepaCoDe, ANR-11-BS09-018), the Chair of Excellence Closed-loop control of turbulent shear flows using reduced-order models (TUCOROM, ANR-10-CHEX-0015), both supported by the French Agence Nationale de la Recherche (ANR) and hosted by Institute PPRIME, the Collaborative Research Center (CRC 880) 'Fundamentals of High Lift for Future Civil Aircraft' funded by the German Research Foundation (DFG) and hosted at the Technical University of Braunschweig, Germany, and the project "Novel Method of Physical Modal Basis Generation for Reduced Order Flow Models" funded by the Polish National Centre of Science under research grant no. 2011/01/B/ST8/07264. EK also thanks for the great support through the region Poitou-Charentes, the NSF PIRE Grant OISE-0968313, and the Air Force research lab under grant AFRL FA8651-16-1-0003. We appreciate valuable stimulating discussions with: Bing Brunton, Steven Brunton, Eric Deem, Nicolai Kamenzky, Nathan Kutz, and Robert Niven.

A Discrete domain decomposition using cluster analysis

Cluster analysis is a part of machine learning and pattern recognition [5] which learns automatically from data. The aim of cluster analysis is to find a hidden grouping among a given set of observations $\{\mathbf{a}^m\}_{m=1}^M$. Here, k-means clustering [25] is employed which groups *kinematically* similar flow states into a low number N_a of clusters \mathcal{A}_i , $i = 1, \dots, N_a$, such that the similarity of observations in the same cluster is maximized while the similarity of observations belonging to different clusters shall be minimized. Here, the *dissimilarity* between observations \mathbf{a}^m and \mathbf{a}^n is measured using the Euclidean distance

$$D(\mathbf{a}^m, \mathbf{a}^n) := \|\mathbf{a}^m - \mathbf{a}^n\|_2. \quad (27)$$

The cluster centroid \mathbf{A}_i of \mathcal{A}_i is defined as the average of observations belonging to the cluster $\mathbf{A}_i := \frac{1}{n_i} \sum_{\mathbf{a}^m \in \mathcal{A}_i} \mathbf{a}^m$ where n_i is the total number of observations in cluster \mathcal{A}_i . The quality of the algorithm is monitored by the total cluster variance, $J_{ca}(\mathbf{A}_1, \dots, \mathbf{A}_{N_a}) = \sum_{i=1}^{N_a} \sum_{\mathbf{a}^m \in \mathcal{A}_i} \|\mathbf{A}_i - \mathbf{a}^m\|_{\mathcal{A}}^2$. The algorithm starts with an initial set of centroids and then iteratively improves them by minimizing the total cluster variance. The set of optimal centroids is thus the solution of the optimization problem

$$\mathbf{A}_1^{opt}, \dots, \mathbf{A}_{N_a}^{opt} = \arg \min_{\mathbf{A}_1, \dots, \mathbf{A}_{N_a}} J(\mathbf{A}_1, \dots, \mathbf{A}_{N_a}). \quad (28)$$

The reader is referred to [23] for more details.

B Control-oriented cluster-based reduced-order model

The propagator of the Markov model (16) for the coarse-grained dynamics shall be directly inferred from data. A multidimensional array $\mathbf{Q} \in \mathbb{R}^{N_a \times N_a \times 2}$ of control-dependent transition probabilities is constructed with elements

$$\mathbf{Q}_{ijb} := \frac{\text{card}\{\mathbf{a}^m | \mathbf{a}^m \in \mathcal{A}_j \text{ and } \mathbf{a}^{m+1} \in \mathcal{A}_i \text{ and } b^m\}}{\text{card}\{\mathbf{a}^m \in \mathcal{A}_j\}} = \text{Prob}(\alpha^{t+1} | \alpha^t, b^t) \quad (29)$$

where card denotes cardinality. The element \mathbf{Q}_{ijb} constitutes the conditional probability that at time $t+1$ the trajectory is in cluster \mathcal{A}_i under the condition that at the previous time step t the trajectory was in cluster \mathcal{A}_j and control b was applied. Array \mathbf{Q} is directly inferred from data based on the relative frequencies of cluster transitions. The control-oriented cluster transition matrix (CTM) \mathbf{P}_κ for a particular control law κ is constructed from the data array \mathbf{Q}_{ijb} as

$$\mathbf{P}_\kappa := [\mathbf{q}_{1\kappa(1)} \cdots \mathbf{q}_{j\kappa(j)} \cdots \mathbf{q}_{N_a\kappa(N_a)}]. \quad (30)$$

with $\mathbf{q}_{j\kappa(j)} = [\mathbf{Q}_{1j\kappa(j)}, \dots, \mathbf{Q}_{N_a j\kappa(j)}]^T$ by selecting the columns $\mathbf{q}_{j\kappa(j)}$ specified by the control law κ . In the following, the temporal evolution of a general cluster probability vector $\mathbf{p} = [p_1, \dots, p_{N_a}]^T$ is pursued. Having an initial probability distribution \mathbf{p}^0 , the cluster probability vector at time t is compactly given by

$$\mathbf{p}^t = \mathbf{P}_\kappa^t \mathbf{p}^0, \quad (31)$$

where the dynamics are prescribed by \mathbf{P}_κ following a particular control law κ . The cluster probability vector has non-negative probabilities, i.e. $p_i^t \geq 0$, and fulfils the normalization condition $\sum_{i=1}^{N_a} p_i^t = 1$ for each timestep t . The long-term behaviour can be studied by powers of the CTM as defined in (31). The asymptotic probability distribution is obtained by

$$\mathbf{p}^\infty := \lim_{t \rightarrow \infty} \mathbf{P}_\kappa^t \mathbf{p}^0. \quad (32)$$

If \mathbf{p}^t converges to a unique, stationary probability vector, the system can be said to be *ergodic*, in the sense that it will be probabilistically reproducible: regardless of the initial region of state space in which it is sampled, the ensemble mean will converge in the infinite-time limit to the time mean.

Each propagator \mathbf{P}_κ defines a time-homogeneous Markov chain with well-known properties [29]: (i) The propagator \mathbf{P}_κ is a stochastic matrix with non-negative elements, i.e. $\mathbf{P}_{ij} \geq 0 \forall i, j$. The elements of each column sum up to unity, i.e. $\sum_{i=1}^{N_a} \mathbf{P}_{ij} = 1 \forall j$. These properties preserve the normalization condition of the probability vector. (ii) The sequence of probability vectors \mathbf{p}^t , $t = 0, 1, 2, \dots$, has no long-term memory. The state at iteration $t+1$ only depends on the t th state and not on any previous iterations. (iii) The absolute values of all eigenvalues of this matrix do not exceed unity. This excludes a diverging vector sequence. (iv) It exists an eigenvalue $\lambda_1(\mathbf{P}_\kappa) = 1$ with algebraic multiplicity 1 and all other eigenvalues satisfy $|\lambda_i(\mathbf{P}_\kappa)| < 1$ for $i = 2, \dots, N_a$. This is a consequence of the Perron-Frobenius theory for non-negative matrices [29]. The eigenvector \mathbf{p}^{*1} associated with the dominant eigenvalue $\lambda_1(\mathbf{P}_\kappa)$ fulfils the fixed-point equation $\mathbf{P}_\kappa \mathbf{p}^{*1} = \mathbf{p}^{*1}$. Since $|\lambda_i(\mathbf{P}_\kappa)| < 1$ for $i = 2, \dots, N_a$, the vector \mathbf{p}^{*1} is the only one that survives infinite iterations. Mathematically, the stationary probability vector \mathbf{p}^∞ must be identical with the eigenvector \mathbf{p}^{*1} associated with the dominant eigenvalue $\lambda_1 = 1$, and thus is a fixed point to (31) for any t . If, however, \mathbf{p}^∞ is oscillatory or non-stationary, the system will not be probabilistically reproducible, displaying a more complicated connection between the initial sampling region and its convergence properties.

C Visualization of control laws

For the purpose of visualizing the similarity of the control laws, a distance matrix \mathbf{D}

$$\mathbf{D}_{ij} = \sqrt{\frac{1}{2} \sum_{t=1}^T (b_i(\mathbf{s}_i(t)) - b_j(\mathbf{s}_i(t)))^2 + \frac{1}{2} \sum_{t=1}^T (b_i(\mathbf{s}_j(t)) - b_j(\mathbf{s}_j(t)))^2} \quad (33)$$

is defined. The $b_i(\mathbf{s}_i(t)) := \kappa^i(\mathbf{s}_i(t))$ is the time series of the control input based on sensor readings \mathbf{s}_i when applying control law κ^i . The time series $b_i(\mathbf{s}_j(t)) := \kappa^i(\mathbf{s}_j(t))$ is obtained from evaluating κ^i using sensor readings \mathbf{s}_j which are collected when κ^j was applied. This permutation is incorporated to ensure the symmetry of \mathbf{D} . Note that $\mathbf{s} = \mathbf{a}$ in the case of full-state information.

A simple method that optimally preserves the control laws' pointwise distances in a least-mean-square-error sense is *multidimensional scaling* (MDS) [28, 14]. For a given distance matrix according to a (possibly non-Euclidean) distance metric, MDS aims to find corresponding points in a low-dimensional subspace so that the distances between the points are preserved. In particular, a two-dimensional subspace denoted by γ_1 and γ_2 for visualization purposes is of interest. The solution can vary in terms of a translation, a rotation and reflections. In the case where the distance is measured via the Euclidean metric, this method coincides with the POD, and the mean is at the origin and the axes are the POD eigenvectors [14].

References

1. Afanasiev, K.: Stabilitätsanalyse, niedrigdimensionale modellierung und optimale kontrolle der kreiszylinderumströmung (trans.: Stability analysis, low-dimensional modeling, and optimal control of the flow around a circular cylinder). Ph.D. thesis, Fakultät Maschinenwesen, Technische Universität Dresden (2003)
2. Bao, F., Dallmann, U.C.: Some physical aspects of separation bubble on a rounded backward-facing step (physikalische phänomene von ablöseblasen an einer abgerundeten zurückspringenden stufe). Aerospace Science and Technology **8**, 83–91 (2004)

3. Bellman, R.E.: Adaptive Control Processes. Princeton University Press, New York (1961)
4. Bertsekas, D.P.: Dynamic Programming and Optimal Control, Vol. II, 4th edn. Athena Scientific (2012)
5. Bishop, C.M.: Pattern Recognition and Machine Learning. Springer, New York (2007)
6. Bollt, E.M., Santitissadeekorn, N.: Applied and Computational Measurable Dynamics. SIAM (2013)
7. Brockett, R.: Notes on the control of the Liouville equation. In: P. Cannarsa, J.M. Coron (eds.) Control of Partial Differential Equations. Cetraro, Italy 2010. Springer-Verlag, Berlin Heidelberg (2012)
8. Brockett, R.W.: Minimizing Attention in a Motion Control Context. Proceedings of the 42nd IEEE Conference on Decision and Control **3349–3352** (2003). Maui, Hawaii USA
9. Brockett, R.W.: On the control of a flock by a leader. In: Proceedings of the Steklov Institute of Mathematics, vol. 268, pp. 49–57 (2010)
10. Brunton, B.W., Brunton, S.L., Proctor, J.L., Kutz, J.N.: Optimal sensor placement and enhanced sparsity for classification. arXiv: 1310.2417 (2015)
11. Brunton, S.L., Noack, B.R.: Closed-loop turbulence control: Progress and challenges. Appl. Mech. Rev. **67**(5), 050,801:01–48 (2015)
12. Brunton, S.L., Proctor, J.L., Kutz, J.N.: Discovering governing equations from data: Sparse identification of nonlinear dynamical systems. arXiv: 1509.03580 (2015)
13. Brunton, S.L., Proctor, J.L., Tu, J.H., Kutz, J.N.: Compressive sampling and dynamic mode decomposition. To appear in J. Comp. Dynamics (2015)
14. Cox, T.F., Cox, M.A.A.: Multidimensional Scaling, *Monographs on Statistics and Applied Probability*, vol. 88, 2nd edn. Chapman and Hall (2000)
15. Duriez, T., Parezanovic, V., Laurentie, J.C., Fourment, C., Delville, J., Bonnet, J.P., Cordier, L., Noack, B.R., Segond, M., Abel, M.W., Gautier, N., Aider, J.L., Raibaud, C., Cuvier, C., Stanislas, M., Brunton, S.L.: Closed-loop control of experimental shear layers using machine learning (invited). AIAA Paper (2014). 7th AIAA Flow Control Conference, Atlanta, Georgia
16. Froyland, G.: Extracting dynamical behavior via markov models. In: A.I. Mees (ed.) Nonlinear Dynamics and Statistics, pp. 281–321. Birkhäuser Boston (2001)
17. Gautier, N., Aider, J.L., Duriez, T., Noack, B.R., Segond, M., Abel, M.W.: Closed-loop separation control using machine learning. Journal of Fluid Mechanics **770**, 242–441 (2015)
18. Ho, C.M., Huerre, P.: Perturbed free shear layers. Ann. Rev. Fluid Mech. **16**, 365–424 (1984)
19. Holmes, P., Lumley, J.L., Berkooz, G., Rowley, C.W.: Turbulence, Coherent Structures, Dynamical Systems and Symmetry, 2nd paperback edn. Cambridge University Press, Cambridge (2012)
20. Hood, P., Taylor, C.: Finite Element Methods in Flow Problems, chap. NavierStokes equations using mixed interpolation, pp. 121–132. University of Alabama in Huntsville Press (1974)
21. Hopf, E.: Statistical hydromechanics and functional analysis. J. Rat. Mech. Anal. **1**, 87–123 (1952)
22. Iversion, K.E.: A Programming Language, 2nd edn. John Wiley & Sons Inc (1962)
23. Kaiser, E., Noack, B.R., Cordier, L., Spohn, A., Segond, M., Abel, M., Daviller, G., Östh, J., Krajnović, S., Niven, R.K.: Cluster-based reduced-order modelling of a mixing layer. J. Fluid Mech. **754**, 365–414 (2014)
24. Lasota, A., Mackey, M.C.: Chaos, Fractals, and Noise, 2nd edn. Springer New York (1994)
25. Lloyd, S.: Least squares quantization in PCM. IEEE Trans. Inform. Theory **28**, 129–137 (1956). Originally as an unpublished Bell laboratories Technical Note (1957)
26. Lorenz, E.N.: Deterministic nonperiodic flow. J. Atm. Sci. **20**, 130–141 (1963)
27. Majumdar, A., Vasudevan, R., Tobenkin, M.M., Tedrake, R.: Convex Optimization of Nonlinear Feedback Controllers via Occupation Measures. International Journal of Robotics Research **33**, 1209–1230 (2014)
28. Mardia, K.V., Kent, J.T., Bibby, J.M.: Multivariate Analysis. Academic Press (1979)
29. Meyer, C.D.: Matrix Analysis and Applied Linear Algebra. Society for Industrial and Applied Mathematics (2000)
30. Morzyński, M.: Numerical solution of navier-stokes equations by the finite element method. In: Proceedings of SYMKOM 87, Compressor and Turbine Stage Flow Path – Theory and Experiment, pp. 119–128 (1987)
31. Munowitz, M., Pines, A., Mehring, M.: Multiple-quantum dynamics in NMR: A directed walk through Liouville space. J. Chem. Phys. **86**, 3172–3182 (1987)
32. Noack, B.R., Niven, R.K.: Maximum-entropy closure for a Galerkin system of incompressible shear flow. J. Fluid Mech. **700**, 187–213 (2012)
33. Sommer, F.: Mehrfachlösungen bei laminaren strömungen mit druckinduzierter ablösung: eine kusen-katastrophe (transl.: Multiple solutions of laminar flows with pressure induced separation: a cusp catastrophe). Tech. Rep. 7:206, Fortschrittberichte VDI, VDI Verlag, Düsseldorf (1992)
34. Sutton, R.S., Barto, A.G.: Reinforcement Learning: An Introduction. MIT Press, Cambridge, MA (1998)
35. Ulam, S.: Problems in Modern Mathematics. Interscience (1964)
36. Wahde, M.: Biologically Inspired Optimization Methods: An Introduction. WIT Press (2008)